Identifying Control Effectiveness Models of the Flying V Sub-Scale Aircraft in the Wind Tunnel Using Multisine Inputs for System Excitation

Saify, B.; de Visser, C.C.; Wang, Xuerui

DOI
10.2514/6.2025-0005

Publication date
2025

Document Version
Final published version

Published in
Proceedings of the AIAA SCITECH 2025 Forum

AIAA SciTech Forum
6-10 January 2025, Orlando, FL
AIAA SCITECH 2025 Forum

10.2514/6.2025-0005

Identifying Control Effectiveness Models of the Flying V Sub-Scale Aircraft in the Wind Tunnel using Multisine Inputs for System Excitation

B. Saify*, C.C. de Visser† and X. Wang ‡
TU Delft Faculty of Aerospace Engineering Kluyverweg 1, Delft, South Holland, 2629HS

Identifying individual control effectiveness parameters for aircraft with several distributed control surfaces can be efficiently performed using multisine inputs. While commonly used in flight testing, these inputs were used to identify control effectiveness models for the half version of the subscale Flying V aircraft through wind tunnel experiments, and these were compared with control effectiveness parameters obtained from static deflections. The control effectiveness parameters estimated through multisine inputs were consistently higher than those obtained from static deflections. This occurs due to inertial forces induced by structural vibrations of the wing in the airstream as the multisine excitation frequency approaches the first natural frequency of the wing. The effects of inertial forces when using multisine inputs are not highlighted in the literature, and bring important consequences for using these inputs on flexible aircraft and wings.

I. Nomenclature

A	=	amplitude of oscillation
C_m	=	pitching moment coefficient
$C_{m_{\delta_i}}$	=	pitching moment control effectiveness for surface with index i
C_L	=	lift coefficient
$C_{L_{\delta_i}}$	=	Lift control effectiveness for surface with index i
δ_i	=	deflection of control surface i in degrees
A_k	=	amplitude of the k^{th} multisine component
ϕ_k	=	phase of the k^{th} multisine component
T	=	period of a multisine input

II. Introduction

Multisines are efficient inputs to excite aircraft dynamics for system identification. In particular, for aircraft with several control surfaces for which individual control effectiveness terms are required, multisines can excite the surfaces simultaneously, yet in an uncorrelated manner [1–7]. The Flying V, developed at TU Delft, is an example of such an aircraft. The Flying V is a flying-wing concept, with distributed control surfaces in the form of six elevons (three on each wing) used primarily for pitch and roll authority and two rudders (one on each winglet) providing yaw authority. Detailed control effectiveness models derived from flight testing and system identification are required for simulation and control system design for this aircraft.

Although multisine inputs offer an efficient solution to identify control effectiveness models for the Flying V subscale flight demonstrator, these inputs were first tested in the wind tunnel using the half-aircraft version of the sub-scale flight test article, shown in Figure 1. The half-aircraft wind tunnel version of the subscale Flying V will be called the Half-V hereon. This wind tunnel test was conducted in December 2023 at the Open Jet Facility (OJF)* at TU Delft.

*PhD Candidate, Aerospace Structures and Materials, b.saify@tudelft.nl
†Associate Professor, Control&Operations
‡Assistant Professor, Aerospace Structures and Materials
*https://www.tudelft.nl/lr/organisatie/afdelingen/flow-physics-and-technology/facilities/low-speed-wind-tunnels/open-jet-facility

Ruiz-Garcia et al. [8] have also conducted static experiments on the Half-V to obtain control effectiveness models followed by flight testing of the Flying V sub-scale model where 3211 and doublet maneuvers were used to identify aerodynamic models from flight test data [9].

In addition to multisine inputs, regular static deflections of the elevons were conducted such that various combinations of elevon positions could be reached to compare the control effectiveness parameters obtained from the multisine inputs with a ground-truth case. Discrete sine sweep maneuvers where all the elevons moved in unison were also utilized. The sine sweeps allowed for finer steps in frequency to study the effects of input frequency on parameter estimates. The control effectiveness parameters were estimated in the time domain for all input types used.

An interesting finding from the multisine maneuvers tested in the wind tunnel was that control effectiveness parameters estimated from the data seemed to depend on the frequency of control surface excitation. Speculating that aeroelastic vibrations of the wing caused this phenomenon, a ground vibration test (GVT) was conducted on the Half-V to characterize the structural dynamic properties of the wing and to use this data to build a simple state space model to analyze the effect of inertial forces on force balance measurements. Finally, a shorter wind tunnel campaign was conducted in November 2024 where the motion of the wing was tracked using the Optitrack system present in the OJF as shown in Figure 1 to understand further how the wing vibrates with wind present.

The paper is outlined as follows. section III describes the methodology for performing the various control surface excitations, control effectiveness parameter estimation, and the experimental setups in the OJF and for the GVT. The wind tunnel campaign and the GVT results are discussed in section IV. The investigation of interesting findings of using multisine maneuvers is discussed in section V. Finally the paper is concluded in section VI

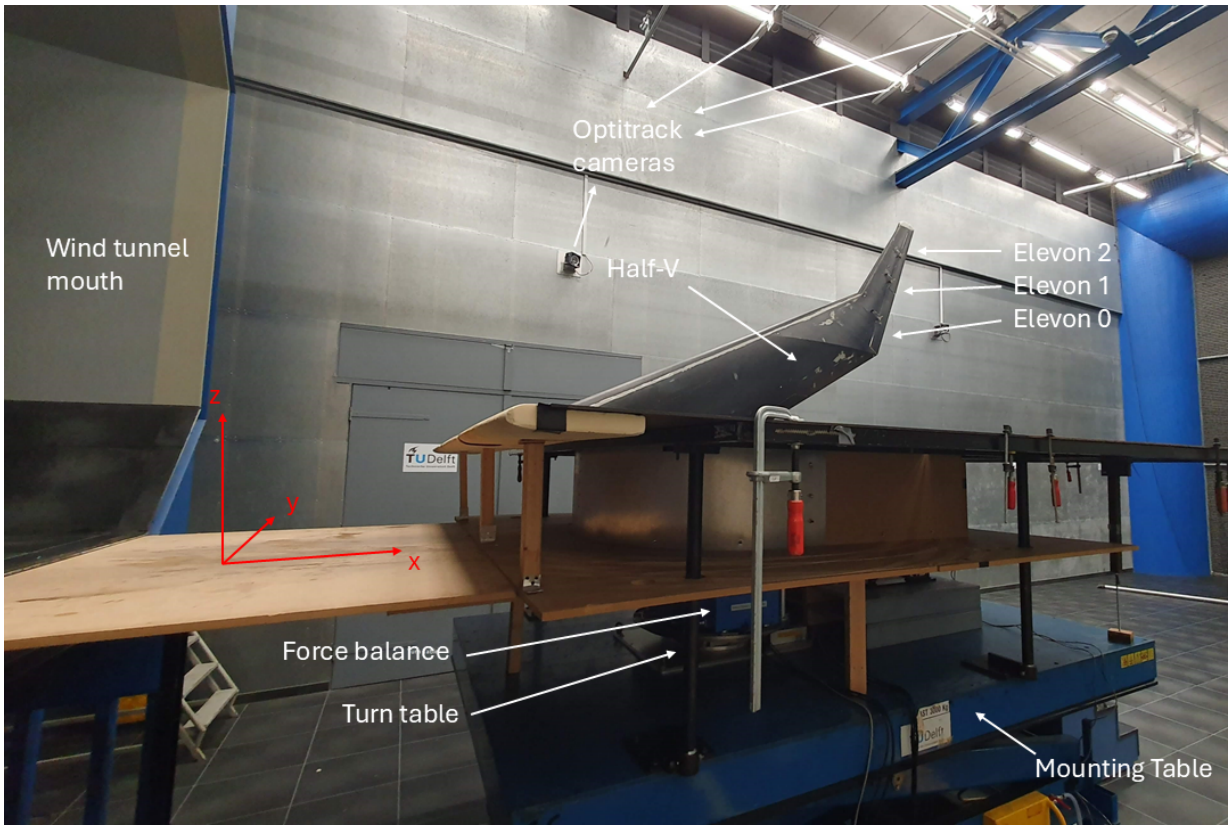

Fig. 1 Experimental setup of the Half-V mounted on the test rig, consisting of a turntable, a force balance, and construction to support the wing and isolate measurement and mounting equipment from the airflow.

III. Methodology

A. Parameter Estimation

The objective of the experimental campaign was to compare the effectiveness of using multisine inputs for identifying individual-surface control effectiveness models of the Half-V with static control surface deflections. The model structure of the pitching moment model, for example, is given by Equation 1. The pitching moment coefficient is a function of the deflections δ_i $i = 0, 1, 2$ of the elevons. The index 0 refers to the inboard elevon, 1 the middle elevon, and 2 the outboard elevon. The parameters to be determined for this linear model are the control effectiveness terms corresponding to each elevon $C_{m_{\delta_i}}$ $i = 0, 1, 2$ which physically represent the contribution of each elevon to producing aerodynamic pitching moment. Dynamic derivatives such as C_{m_q} are not included in the model as dynamic motions of the wing could not be excited in the wind tunnel. Additionally, the results shown in this paper are at a single angle of attack (0 degrees), hence the C_{m_α} parameter is also omitted. Equation 2 is used to model the aerodynamic lift and the contribution of each elevon to lift generation ($C_{L_{\delta_i}}$) in a similar manner to the pitching moment model in Equation 1.

$$C_m = C_{m_0} + C_{m_{\delta_0}}\delta_0 + C_{m_{\delta_1}}\delta_1 + C_{m_{\delta_2}}\delta_2 \tag{1}$$

$$C_L = C_{L_0} + C_{L_{\delta_0}}\delta_0 + C_{L_{\delta_1}}\delta_1 + C_{L_{\delta_2}}\delta_2 \tag{2}$$

The various control effectiveness parameters were estimated using an Ordinary Least Squares (OLS) estimator in the time domain. The explanatory variables are the measured angles of the control surfaces (δ_i) and the modeled variables are the measured non-dimensionalized pitching moment and lift coefficients.

A global linear-in-the-parameters polynomial model, Equation 3, is used to model the dependent variable $\boldsymbol{y} \in \mathbb{R}^n$. This model combines regressors $A = [\ 1 \quad \boldsymbol{\xi 1} \quad \boldsymbol{\xi 2} \quad \dots \quad \boldsymbol{\xi_p}\ ] \in \mathbb{R}^{n\times p}$ with model parameters $\boldsymbol{\theta} \in \mathbb{R}^p$ and residuals $\boldsymbol{\epsilon} \in \mathbb{R}^n$. The optimal parameters $\hat{\boldsymbol{\theta}}$ are determined using an Ordinary Least Squares estimator, Equation 4. The parameter variance-covariance matrix is determined using Equation 5 where σ^2 is the variances of the residuals [10].

$$\boldsymbol{y} = A\boldsymbol{\theta} + \boldsymbol{\epsilon} \tag{3}$$

$$\hat{\boldsymbol{\theta}} = \left(A^T A\right)^{-1} A^T \boldsymbol{y} \tag{4}$$

$$Cov(\hat{\boldsymbol{\theta}}) = \sigma^2 \left(A^T A\right)^{-1} \tag{5}$$

B. Multisine Inputs

Multisine inputs are a sum of sine waves with a prescribed amplitude and phase for each frequency component, where all control surfaces simultaneously get a unique multisine command signal. The frequencies of the individual sine waves are chosen such that the correlation between the deflections of the control surfaces is zero. Equation 6 is used to define the deflection δ_i of control surface i as a function of time, where T is the period, n is the total number of frequencies, A_k is the amplitude and ϕ_k the phase[2]. A uniform amplitude spectrum was used, meaning each frequency gets the same amplitude. The phase angles are generally optimized to minimize the relative peak factor (RPF) through a simplex algorithm, however a less optimal set of phases can be recursively created using Equation 7[10].

$$\delta_i = \sum_{k\in 1,2,\dots,n} A_k \sin\left(\frac{2\pi k t}{T} + \phi_k\right) \tag{6}$$

$$\phi_k = \phi_{k-1} - \frac{\pi k^2}{n} \quad k = 2, 3, \dots, n \tag{7}$$

The multisine deflections performed during the wind tunnel testing campaign were varied by adjusting the maximum frequency and the signal amplitude. Due to limitations on the speed of the servos, the maximum frequency used was 3.6 Hz. The period T was chosen to be 5 seconds for all the multisine tests, which sets the lowest frequency at 0.2 Hz which was considered satisfactory in terms of the frequency resolution that can be achieved in separating the individual sine waves for each input. The frequencies were assigned sequentially to ensure a uniform spectral distribution to each of the

surfaces. Additionally, for a single experiment, the same 5-second multisine was repeated 10 times to allow for phase averaging of the data at a later stage to study the noise characteristics.

Figure 3 shows the measured non-dimensionless forces and moments from a multisine input including the full measurement times-series data as well as the phase-averaged data. The amplitude spectra of the measured lift coefficient and measured control surface deflection from the same multisine test are shown in Figure 2. It is clear from the figure that each elevon is assigned four frequencies such that they cover a large portion of the tested spectrum. The maximum frequency in this example was 2.6 Hz, and a minimum of 0.4 Hz. From the amplitude spectra of the lift coefficient, it is clear that the lift force is excited at the same frequencies as the control surfaces. The discrepancy in the heights of the relative peaks in the lift spectra is explained by the fact that the elevons differ in size, the largest being the inboard elevon with the larger peaks and the smallest being the outboard elevon which leads to smaller peaks while the central elevon produces peaks in between the other two.

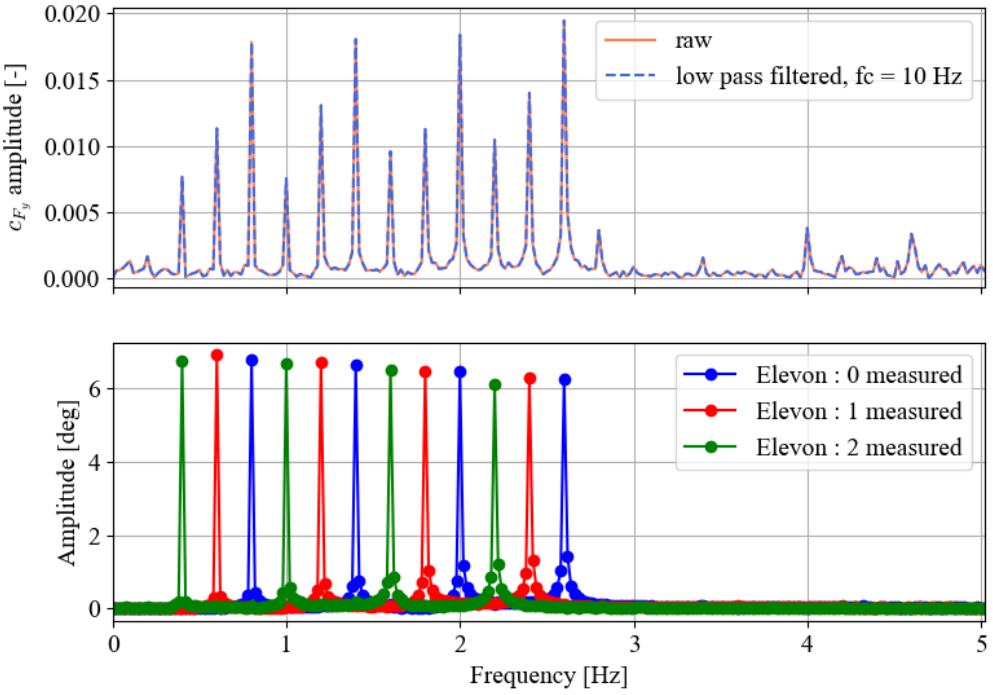

Fig. 2 Amplitude spectra of the measured lift coefficient and the measured deflections of each of the three elevons for a multisine input excitation

C. Static deflections

Static deflections were performed where the elevons were each deflected simultaneously to a particular angle and held for 5 seconds. Each elevon was deflected from -10 degrees to +10 degrees in steps of 5 degrees, resulting in 125 total deflection combinations for the tested elevons. Therefore, a single run for the static deflection maneuver lasted about 10 minutes, compared to 50 seconds for the multisine tests. The control effectiveness parameters estimated using static deflections as inputs serve as a ground-truth case to compare the parameters estimated using multisine inputs.

D. Discrete Sine Sweep Inputs

In addition to the static deflection and multisine inputs, discrete sine sweeps were also tested. However, in this case, the three elevons were moved in unison. Therefore, the individual control effectiveness contributions of each eleven cannot be captured through these inputs. Instead, the control effectiveness parameters estimated from this input combine

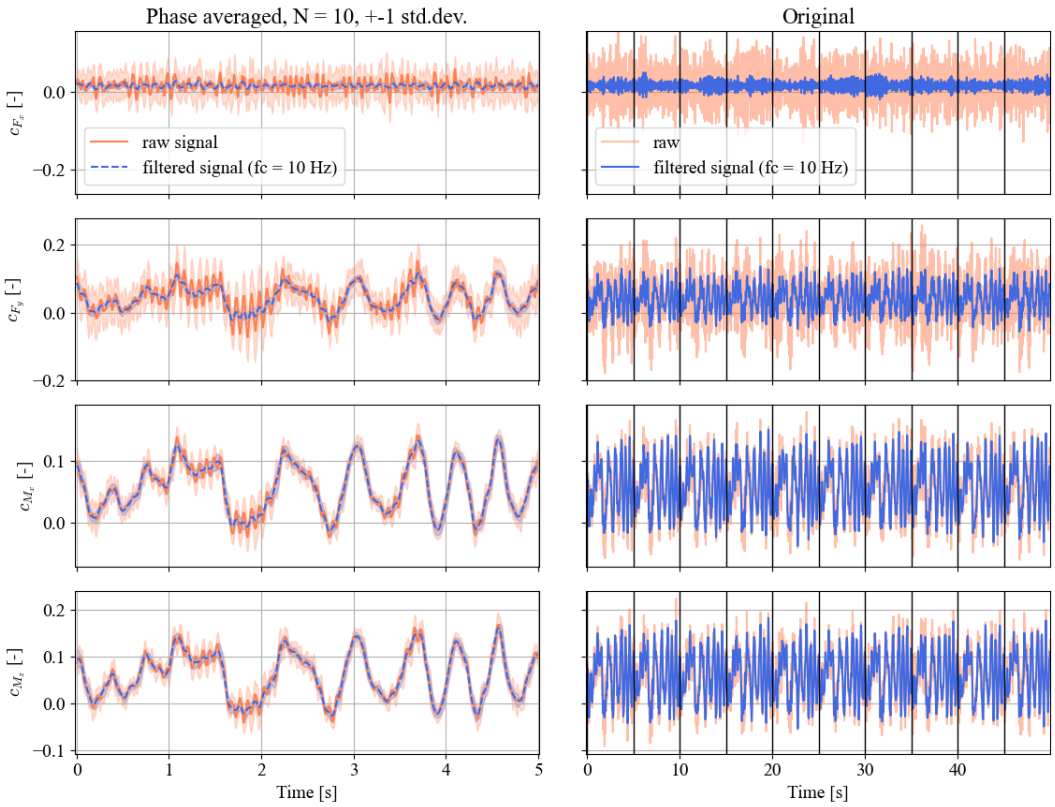

Fig. 3 Example of the non-dimensionalized time series measurements of the force balance from a multisine input. The right column shows plots of the complete measurement in orange and the low pass filtered measurement in blue, while the left column is the phase-averaged version of the corresponding plot on the same row

the surfaces into one equivalent elevon. The purpose of these inputs was to see if, and how control effectiveness varies with the frequency of control surface excitation. The discrete sine sweep inputs consisted of sequential 10-second long intervals, starting at a frequency of 0.5 Hz and going up to 2.5 Hz in steps of 0.25 Hz.

E. Wind Tunnel Setup

The OJF is a large low-speed wind tunnel that can produce steady wind at up to 35 [m/s] and features a nozzle with dimensions 2.85 x 2.85 m. For the experimental runs performed in the current work, the maximum airspeed reached was 25 m/s.

The experimental setup shown in Figure 1 consists of the Half-V and the surrounding structure on which it is mounted. The force balance measures forces and moments and is mounted on a turn-table which can be used to set the incidence angle of the wing to the airflow coming from the wind tunnel. The forces and moments are measured at a frequency of 2 kHz and recorded on a PC.

An Arduino Uno [†] housed inside the Half-V is used to generate the input signals and send these to the elevon servos. The shafts of each of the three elevon servos are connected to potentiometers which are used to measure the angle reached by each control surface. Due to kinematic non-linearities in the linkages connecting the control surfaces and servo axes, polynomial mappings up to third order were created to compute the angle of each surface based on the potentiometer readings. The Arduino Uno reads the potentiometer signals using the analog input pins at around 100 Hz per servo. The analog signals are converted to digital onboard the Arduino and transmitted to a PC connected to the Arduino via a serial link. The data is stored on the PC.

[†] `https://store.arduino.cc/products/arduino-uno-rev3`

F. GVT Setup

The GVT was performed using a Mini SmartShaker modal shaker from The Modal Shop[‡] to excite the structure and a PSV-500 laser scanning vibrometer from Polytec [§] to measure the structural response. The Model 288D01 mechanical impedance sensor from PCB Piezotronics [¶] served to measure the input force acting on the wing through the shaker. The wing is mounted such that it is clamped to an aluminum support frame that is clamped to an optical table. The setup is shown in Figure 4 and Figure 5.

The laser scanning vibrometer scans one point of the structure at a time, with 33 points in total. Each point is scanned with the same excitation given by the shaker such that the different measurements are phase averaged to obtain the final frequency response functions (FRF) of the wing at each scanned point.

The wing was excited using a pseudo-random input with a frequency resolution of 39.0625 mHz, and a sampling rate of 500 Hz leading to 6400 spectral lines in each FRF. This results in the scan time at a single point of 25.6 seconds. However, three measurements were taken per point to calculate averaged FRFs to reduce the effect of noise. The data acquisition and processing is done through software from PSV [‖]

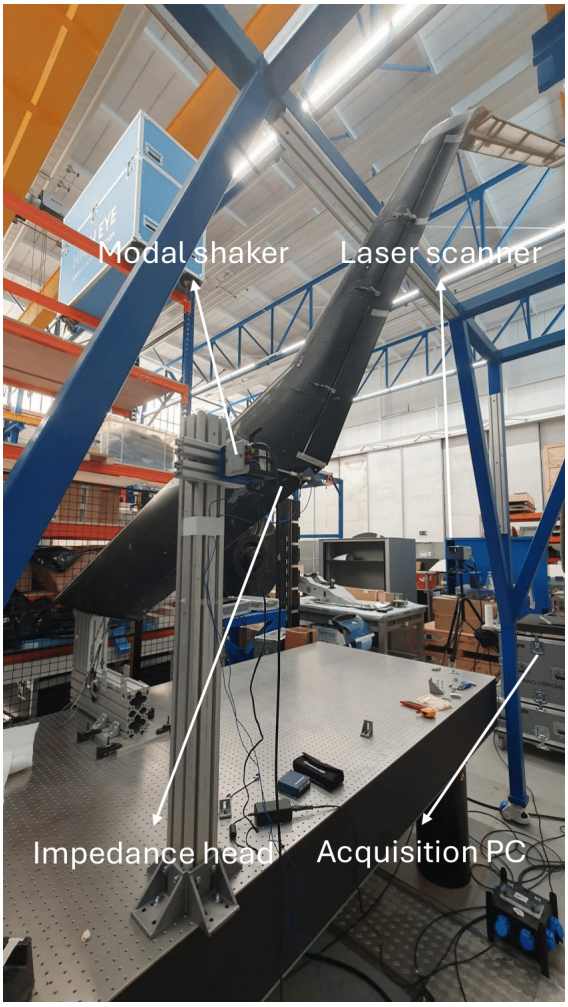

Fig. 4 GVT test setup

Fig. 5 GVT measurement points

[‡] https://www.modalshop.com/vibration-test/products/vibration-test-shakers/smartshaker-integrated-amp
[§] https://www.polytec.com/int/vibrometry/products/full-field-vibrometers/psv-500-scanning-vibrometer
[¶] https://www.pcb.com/products?m=288d01
[‖] https://www.polytec.com/int/vibrometry/products/software/psv-software

IV. Results

A. Wind Tunnel Tests

The results from the initial experimental campaign from December 2023 are shown in Figure 6 and Figure 7. In these figures, the estimates of the longitudinal control effectiveness parameters are plotted, with each value coming from different multisine tests and static deflection tests. An interesting result from these figures is that the parameter estimates obtained from multisine inputs are always higher than those for the static deflection case. Furthermore, the higher the maximum frequency used for a multisine input, the higher the control effectiveness estimates. As explained in later sections, this phenomenon is caused by force balance measurements being corrupted by inertial forces from the vibration of the wing around its natural frequencies which are excited by aerodynamic loads due to control surface deflection as well as stochastic loads caused by turbulence in the airstream.

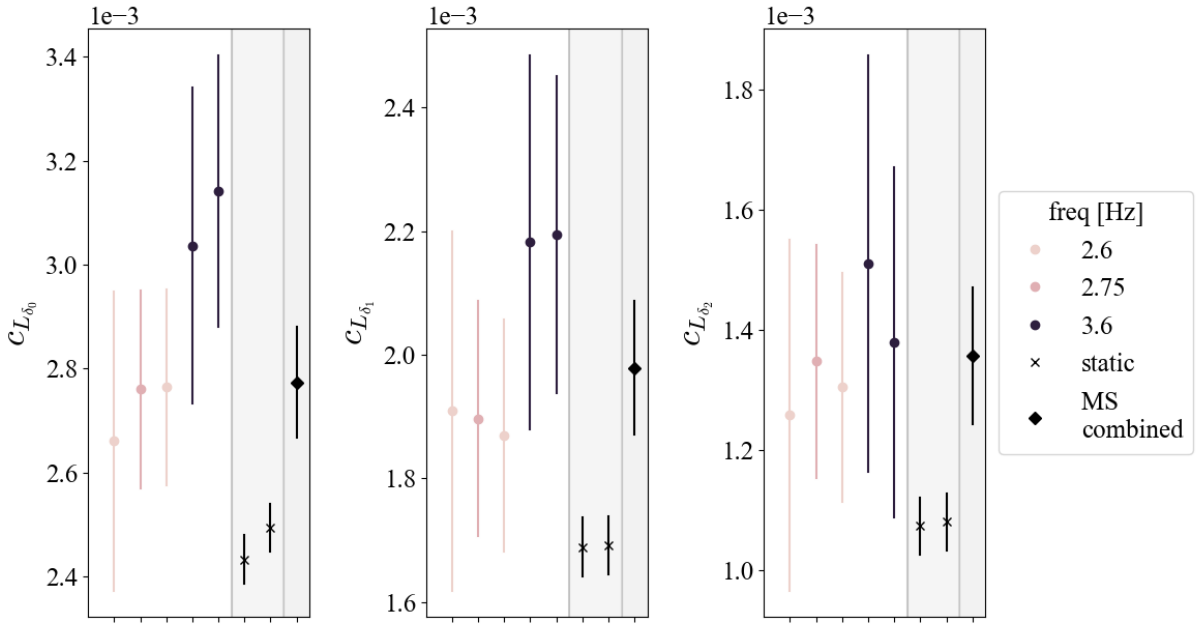

Fig. 6 Comparison of lift control effectiveness parameters for each elevon at varying multisine frequencies, and with static deflection results

The results from the discrete sine sweep inputs further corroborate the control effectiveness increase observed from the multisine inputs. Figure 8 shows the variation of the pitch moment control effectiveness parameters as a function of the frequency used to excite the control surfaces. The plot on the left shows the raw scattered data mapping elevator deflection to the measured non-dimensionalized pitching moment where each frequency is separated by color, and the solid lines indicate a linear fit to the data at each frequency where the slopes of these lines indicate the control effectiveness at that respective frequency. The right plot shows the control effectiveness as a function of the oscillation frequency, these are the slopes of the corresponding lines in the left plot. The vertical bars indicate the 3 times the standard deviation of the parameters based on the parameter variances calculated using Equation 5.

It is reiterated here that the elevons move in unison during the discrete sine sweep input and so the control effectiveness parameter is not for a single elevon but rather the equivalent control effectiveness of a fictitious bigger elevon which is a combination of the three elevons present on the wing.

B. GVT Results

The FRFs obtained from the GVT were analyzed using Siemens Simcenter Testlab. The PolyMAX method was used to extract the system's modal model. A frequency range from 39.0625 mHz up to 50 Hz was used since higher

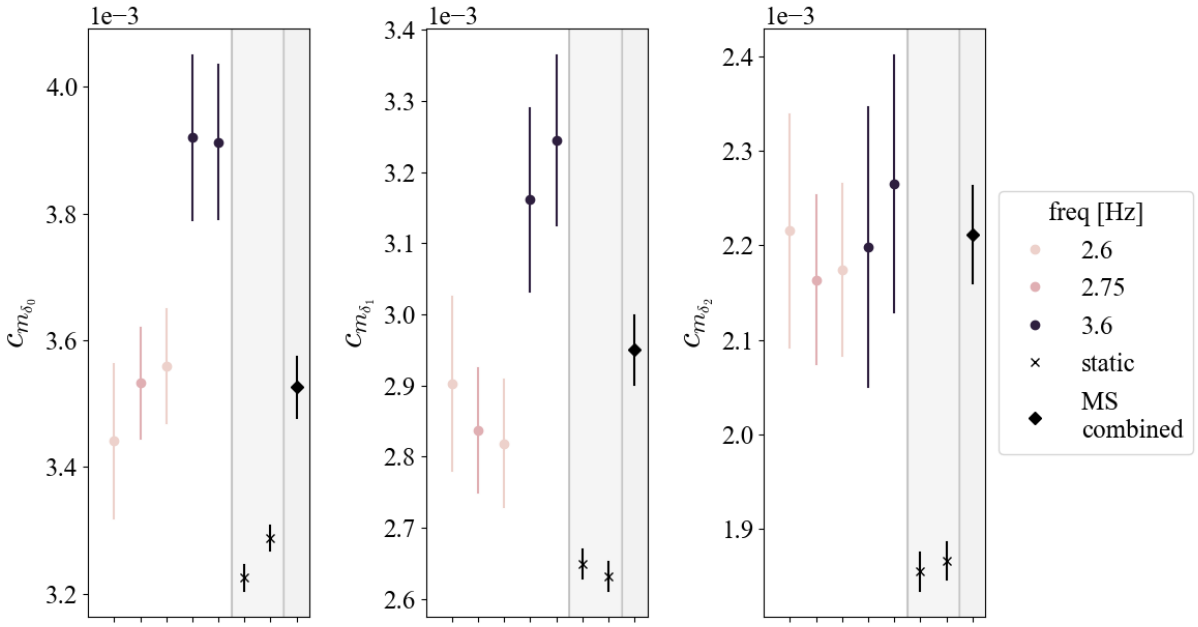

Fig. 7 Comparison of pitch moment control effectiveness parameters for each elevon at varying multisine frequencies, and with static deflection results

Table 1 Modal properties of the Half-V

Mode	Natural Frequency [Hz]	Damping [%]
First bending	6.65	0.84
Second bending	14.65	1.41
First torsion	27.65	2.05

frequency modes were not considered influential for the effects seen in the wind tunnel, which manifested in a frequency range between 0 and 20 Hz.

The modal analysis found four modes of the wing below 50 Hz. However, only the first three are reported here and only the first two are considered important for explaining the phenomenon of apparent control effectiveness increase with excitation frequency described in the previous section. The first three modes and their properties are shown in Table 1. The mode shapes are visualized in Figures 10 to 12.

V. Discussion

From Figure 8, the pitching moment control effectiveness increases by about 13% as the control surface deflection frequency increases from 0.5 Hz to 2.5 Hz. This is because the force balance measurements are affected by the inertial forces imparted on the force balance by the wing and the mount connecting it to the force balance. Additionally, the blue table (see Figure 1) on which the whole setup is mounted was dynamically analyzed by LeBlanc et al. [11] where the side-side rigid body mode of the table was found to occur at 5.82 Hz, with a damping of 1.5% (of the critical damping ratio) and an equivalent spring constant of 2.309e6 N/mm [11]. Therefore, the dynamics of the table may also impact the force balance measurements.

To understand the effects of the structural dynamics of the wing, as well as the blue table, a simple 2-degree-of-freedom (DoF) model was constructed by treating the wing (and its mounting frame) and blue table (including the force balance) as mass-spring-damper systems connected in series to model what the force balance measures when a cyclic

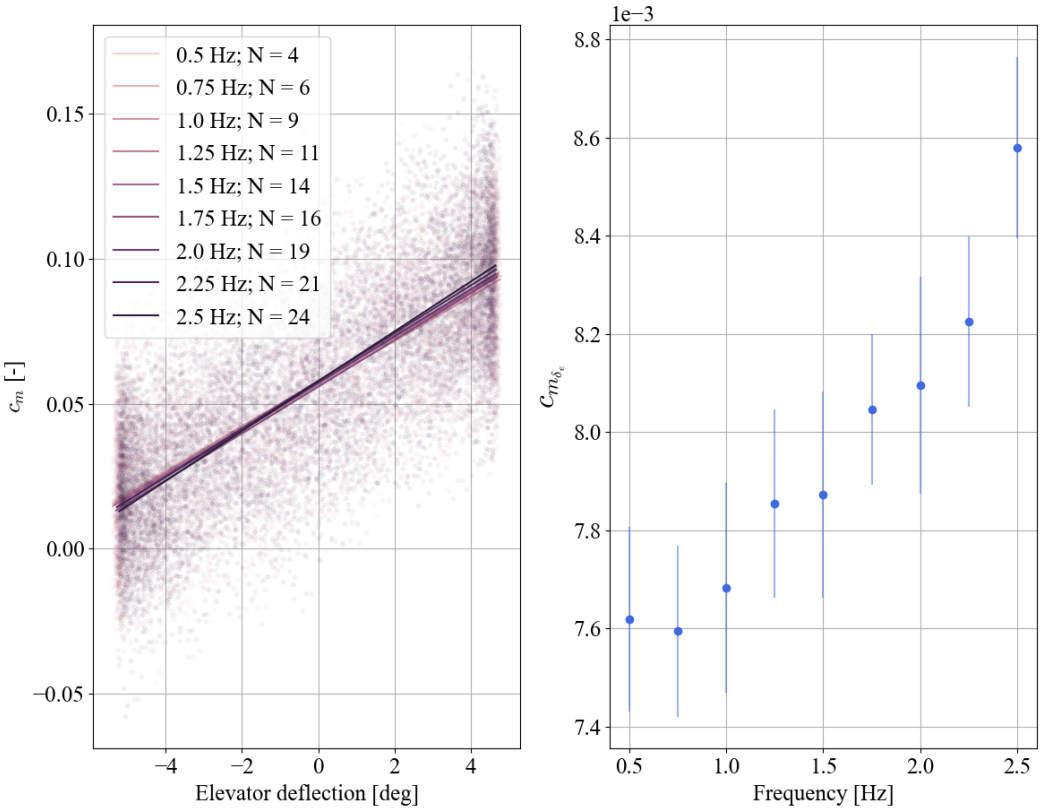

Fig. 8 Variation of the estimated pitching moment control effectiveness with the frequency of control surface excitation where N in the legend signifies the number of sine waves at each frequency.

Table 2 Mass stiffness and damping properties of the wind tunnel setup

m_w	32 kg	k_w	56 kN/m	d_w	0.84 %
m_t	1670 kg	k_t	2309 kN/m	d_t	1.5 %
m_b	55 kg				

load is applied to the wing. In this case, the lift is idealized as a concentrated load. The single-input single-output (SISO) system has the idealized lift as input and the force measured at the force balance as output. The lift measured by the force balance equals the reaction force exerted by the blue table on the balance, which depends on the positions and velocities of the wing and blue table. The state space equations for this idealized 2-degree-of-freedom system are given by Equation 8 and Equation 9 where the former is the equation of state, and the latter is the output equation. The wing and table deflections are represented by states x_1 and x_3 respectively, and the wing and table velocities are represented by states x_2 and x_4 respectively. The input is the idealized concentrated lift on the wing L and the output is the force balance measurement F_b. The parameters m, k, and c refer to mass, spring constant, and damping respectively, and subscripts w, t, and b refer to the wing, table, and force balance respectively. The table's mass, stiffness, and damping properties are taken from [11]. The properties of the wing were found through the GVT. The values of all the parameters are summarized in Table 2. Damping values are computed from the damping ratio and critical damping.

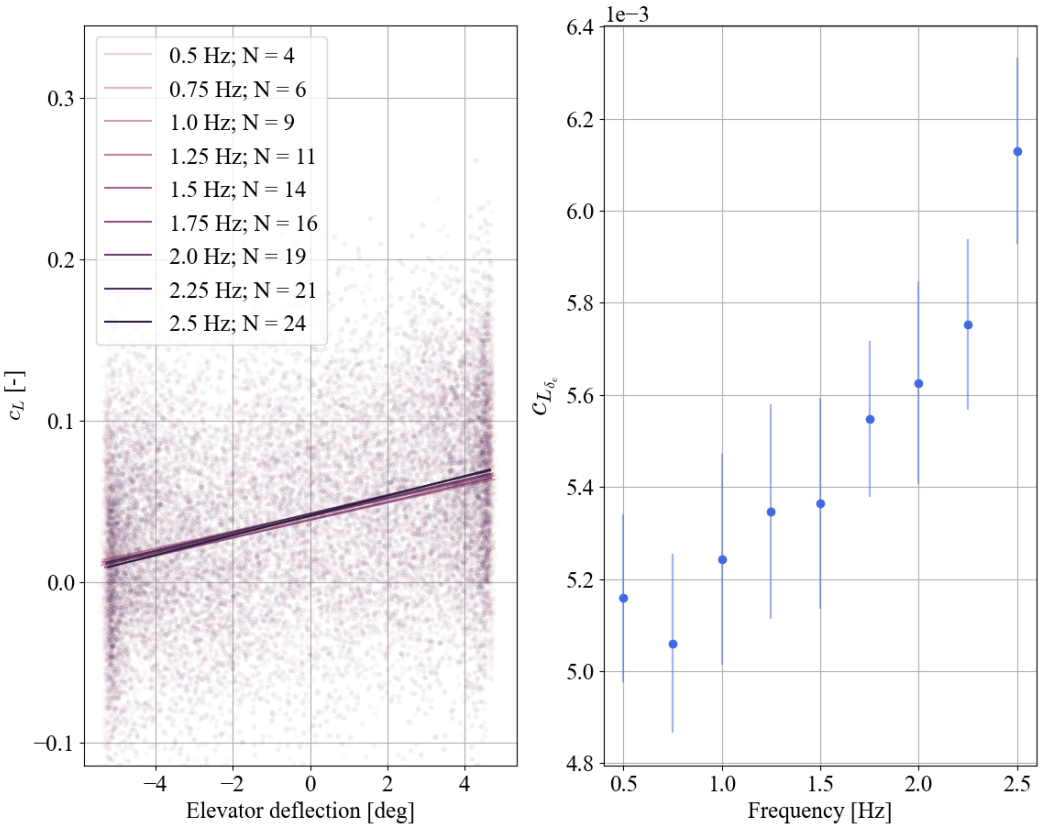

Fig. 9 Variation of the estimated lift control effectiveness with the frequency of control surface excitation where N in the legend signifies the number of sine waves at each frequency.

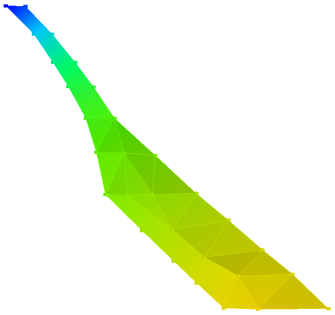

Fig. 10 First bending mode at 6.65 Hz

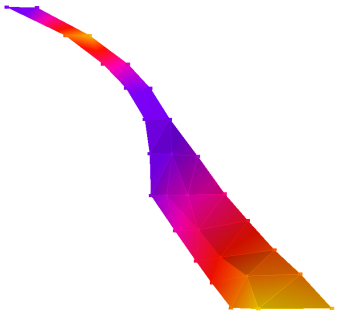

Fig. 11 Second bending mode at 14.65 Hz

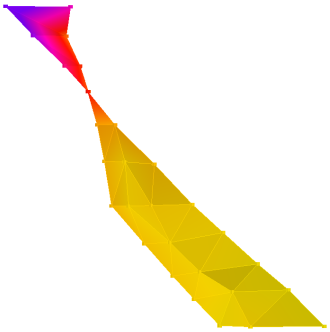

Fig. 12 First torsion mode at 27.65 Hz

$$\begin{bmatrix} \dot{x_1} \\ \dot{x_2} \\ \dot{x_3} \\ \dot{x_4} \end{bmatrix} = \begin{bmatrix} 0 & 1 & 0 & 0 \\ -\frac{k_w}{m_w} & -\frac{c_w}{m_w} & \frac{k_w}{m_w} & \frac{c_w}{m_w} \\ 0 & 0 & 1 & 0 \\ \frac{k_w}{m_b+m_t} & \frac{c_w}{m_b+m_t} & \frac{-k_w-k_t}{m_b+m_t} & \frac{-c_w-c_t}{m_b+m_t} \end{bmatrix} \begin{bmatrix} x_1 \\ x_2 \\ x_3 \\ x_4 \end{bmatrix} + \begin{bmatrix} 0 \\ \frac{1}{m_w} \\ 0 \\ 0 \end{bmatrix} L \tag{8}$$

$$F_b = \begin{bmatrix} \frac{m_t k_w}{m_b+m_t} & \frac{m_t c_w}{m_b+m_t} & \frac{-m_t k_w+m_b k_t}{m_b+m_t} & \frac{-m_t c_w+m_b c_t}{m_b+m_t} \end{bmatrix} \begin{bmatrix} x_1 \\ x_2 \\ x_3 \\ x_4 \end{bmatrix} + \begin{bmatrix} 0 \end{bmatrix} L \tag{9}$$

Figure 13 shows the bode diagram of the above system (green curve), as well as the case where the table is assumed to be rigid (black curve), and where the wing is assumed to be rigid (blue curve). The bode diagram indicates that as the frequency of the input force (Lift) increases, the higher the scale factor error in measuring this force at the force balance up to the first natural frequency of the coupled system. The red crosses show the normalized version of the lift control effectiveness parameters estimated from wind tunnel data from a discrete sine-sweep input shown in Figure 9. The lift-control effectiveness at 0.5 Hz is used as the normalizing quantity.

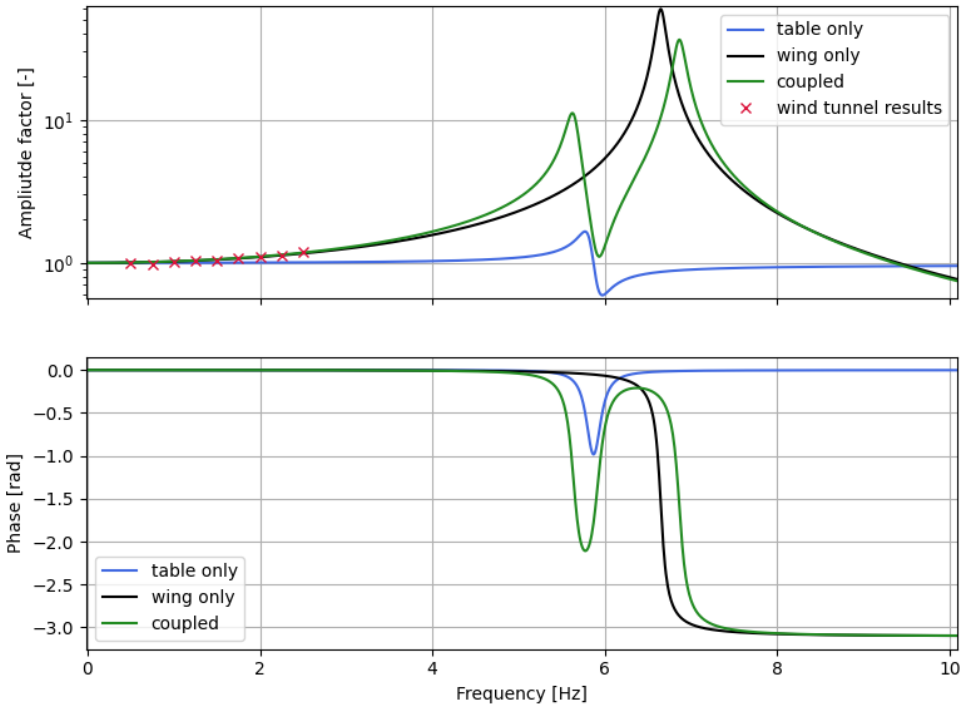

Fig. 13 Bode diagram of the ratio between measured force and the input (lift) force predicted by simplified linear state-space models of the Half-V (black), the mounting table for the experimental setup (blue), and the coupled system (green) where red crosses signify

Figure 13 shows that the increasing control effectiveness observed from wind tunnel data (red crosses) agrees well with the prediction of the simple 2 DoF model which incorporates structural properties of the wing and mounting table obtained through ground vibration testing of these structures. However, it is reiterated here that this model is very simplified. It is assumed that only the first bending mode of the wing is significant, and its modal mass is assumed to be that of the whole wing. Additionally, the lift distribution is concentrated into a point load.

Another important point of discussion is that the force balance measurements from the first wind tunnel campaign in 2023 showed peaks in frequencies that were close to the natural modes of the wing found from the GVT, but consistently slightly lower than the GVT values. Initially, it was assumed that the aeroelastic coupling of the wing in the airstream causes a change in frequencies of the coupled system as a function of airspeed. Therefore, a series of wind tunnel experiments were conducted in December 2024 (with the same setup as the previous test in 2023) where the airspeed was increased from 5 m/s up to 18 m/s, and the wing was allowed to vibrate freely in the airflow with stochastic disturbances due to turbulence in the airstream acting as the excitation. In addition to the force balance measurements, the motion of the wing was also tracked using the Optitrack system in the OJF which provides sub-millimeter spatial resolution and a

sampling rate of up to 360 Hz.

Figure 14 shows that the variation of the frequencies with airspeed is not the cause for the lower modal frequencies observed from force balance data in the wind tunnel. At low airspeeds, the dynamic response should be dominated by the structural dynamics of the wing. However, the frequencies detected in both the force balance and the Optitrack measurements of wing motion are consistently lower than those of the GVT. The source of this discrepancy is therefore likely coming from the part of the force balance which sits on top of the load cells and connects to the wing mount. The mass of this part adds to that of the wing and its mount, therefore effectively lowering the frequencies.

The results presented in Figure 14 also show that the force balance and Optitrack measurements agree in terms of frequencies measured, and so it can also be concluded with confidence that inertial forces due to the motion of the wing cause the force balance readings to be influenced, resulting in artificially increased control effectiveness terms being estimated if this phenomenon is not taken into consideration.

Most existing literature on multisine inputs for aircraft system identification focuses on the flight-test use case, not wind tunnel testing. Inertial forces that affect measurements are a problem when the wing is clamped, as is often the case in a wind tunnel. However, for a flexible free-flying aircraft, the same inertial forces are present, but act to move the c.g. of the aircraft, and the inertial measurement units onboard will capture the resulting specific forces and angular rates. Therefore, when using multisine control surface excitation for flight testing, or especially for wind tunnel testing with a clamped wing, these inertial forces should be accounted for and subtracted from the measurements if possible. In the wind tunnel, a straightforward approach to achieve this would be to use accelerometers mounted to the wing (or another motion capture system such as Optitrack), along with a mass distribution of the wing to subtract the inertial forces from the measurements, an approach that was used by Mertens et al. [12] to subtract the inertial forces from force balance measurements of a highly flexible wing known as the Delft-Pazy wing.

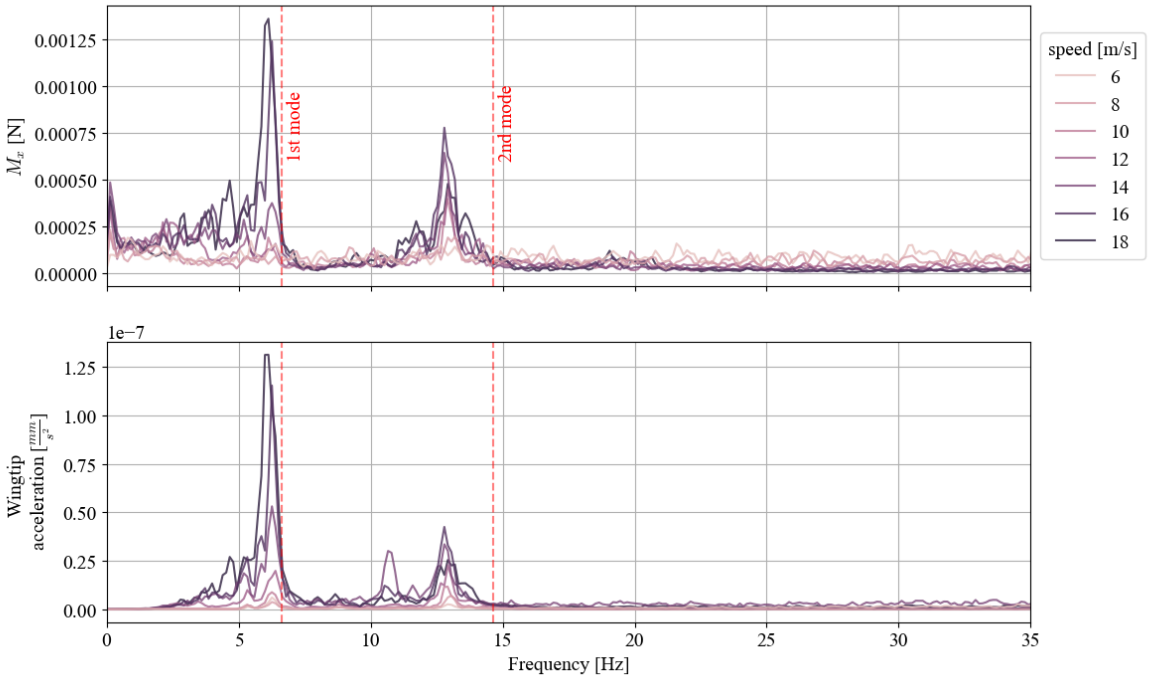

Fig. 14 Power spectra of root bending moment obtained from the force balance and Optitrack wing acceleration measurements at different airspeeds, including the first two modal frequencies of the wing obtained from the GVT shown as red dashed lines

VI. Conclusion

Multisine inputs offer an efficient means of identifying detailed control effectiveness parameters from flight tests and wind tunnel data because all the surfaces can be excited together in an uncorrelated manner. In this paper, multisine inputs were executed on a half-version of the sub-scale Flying. It was found that while these inputs were comparable to static deflections in estimating control effectiveness parameters of control surfaces, the estimates were consistently higher, and were also observed to increase with the multisine input frequency.

It was found that the reason for the apparent control effectiveness increase was from inertial forces due to wing motion being picked up by the force balance and added to the aerodynamic forces generated by the wing and its control surfaces. A simple 2-degree-of-freedom mass spring damper system was used to quantify and model this phenomenon, where the parameters for the model were found experimentally by performing a ground vibration test on the wing. The simple model showed good agreement with wind tunnel data, further giving confidence that the inertial forces are the cause of the apparent control effectiveness increase.

Existing literature on the use of multisines for flight testing and model identification does not explicitly mention the consequences of inertial forces and their effects on parameters estimation [1–7]. The presented work shows that this is an important phenomenon that should be considered carefully, especially when high-frequency multisine inputs are used in wind tunnel and flight testing.

As a next step, multisine inputs will be used to identify models for the sub-scale flight article of the Flying V through flight test data. A variety of input frequencies will be used to test how the parameter estimates are affected, and how they compare with more traditional inputs such as doublets and 3211 inputs.

Acknowledgments

This publication is part of the project Flying V Flight Control with project number 19511 of the research program Open Technology Programme, which is (partly) financed by the Dutch Research Council (NWO). The authors would like to acknowledge the in-kind contribution of KLM Royal Dutch Airlines and ADSE.

References

[1] Morelli, E. A., "Multiple input design for real-time parameter estimation in the frequency domain," *IFAC Proceedings Volumes*, Vol. 36, No. 16, 2003, pp. 639–644.

[2] Morelli, E. A., "Flight test maneuvers for efficient aerodynamic modeling," *Journal of Aircraft*, Vol. 49, American Institute of Aeronautics and Astronautics Inc., 2012, pp. 1857–1867. https://doi.org/10.2514/1.C031699.

[3] Grauer, J. A., and Boucher, M. J., "Aircraft system identification from multisine inputs and frequency responses," *Journal of Guidance, Control, and Dynamics*, Vol. 43, No. 12, 2020, pp. 2391–2398. https://doi.org/10.2514/1.G005131.

[4] Grauer, J. A., and Boucher, M. J., "Real-time estimation of bare-airframe frequency responses from closed-loop data and multisine inputs," *Journal of Guidance, Control, and Dynamics*, Vol. 43, American Institute of Aeronautics and Astronautics Inc., 2020, pp. 288–298. https://doi.org/10.2514/1.G004574.

[5] Morelli, E. A., "Optimal Input Design for Aircraft Stability and Control Flight Testing," *Journal of Optimization Theory and Applications*, Vol. 191, No. 2-3, 2021, pp. 415–439. https://doi.org/10.1007/s10957-021-01912-0.

[6] Morelli, E. A., "Practical Aspects of Multiple-Input Design for Aircraft System Identification Flight Tests," *AIAA Aviation and Aeronautics Forum and Exposition, AIAA AVIATION Forum 2021*, American Institute of Aeronautics and Astronautics Inc, AIAA, 2021. https://doi.org/10.2514/6.2021-2795.

[7] Grauer, J. A., "Frequency Response Estimation for Multiple Aircraft Control Loops Using Orthogonal Phase-Optimized Multisine Inputs," *Processes*, Vol. 10, No. 4, 2022. https://doi.org/10.3390/pr10040619.

[8] Ruiz-García, A., Vos, R., and de Visser, C. C., "Aerodynamic model identification of the flying V from wind tunnel data," *AIAA AVIATION 2020 FORUM*, Vol. 1 PartF, American Institute of Aeronautics and Astronautics Inc, AIAA, 2020. https://doi.org/10.2514/6.2020-2739.

[9] García, A. R., Brown, M., Atherstone, D., Arnhem, N. v., and Vos, R., "Aerodynamic Model Identification of the Flying V from Sub-Scale Flight Test Data," *AIAA Science and Technology Forum and Exposition, AIAA SciTech Forum 2022*, American Institute of Aeronautics and Astronautics Inc, AIAA, 2022. https://doi.org/10.2514/6.2022-0713.

[10] Morelli, E. A., and Klein, V., *Aircraft system identification: theory and practice*, Vol. 2, Sunflyte Enterprises Williamsburg, VA, 2016.

[11] LeBlanc, B., and Ferreira, C., "Experimental characterization of H-VAWT turbine for development of a digital twin," *Journal of Physics: Conference Series*, Vol. 1452, IOP Publishing, 2020, p. 012057.

[12] Mertens, C., Costa Fernández, J. L., Sodja, J., Sciacchitano, A., and van Oudheusden, B. W., "Nonintrusive Experimental Aeroelastic Analysis of a Highly Flexible Wing," *AIAA Journal*, 2023, pp. 1–16. https://doi.org/10.2514/1.j062476.